Phase Stability and Fast Ion Conductivity in the Hexagonal LiBH4-LiBr-LiCl Solid Solution

Phase Stability and Fast Ion Conductivity in the Hexagonal $LiBH_4$-LiBr-LiCl Solid Solution

Valerio Gulino,[a)b)] Matteo Brighi,[b)] Erika M. Dematteis,[a)] Fabrizio Murgia,[b)] Carlo Nervi,[a)] Radovan Černý,[b)] and Marcello Baricco[a)*]

[a)] Department of Chemistry and Inter-departmental Center Nanostructured Interfaces and Surfaces (NIS), University of Turin, Via Pietro Giuria 7, 10125 Torino, Italy

[b)] Laboratoire de Cristallographie, DQMP, Université de Genève, quai Ernest-Ansermet 24, CH-1211 Geneva 4, Switzerland

*Corresponding author

Marcello Baricco

E-mail address: marcello.baricco@unito.it

Tel.: +39 011 6707569

Fax: +39 0116707856

Abstract

This study shows a flexible system that offers promising candidates for Li-based solid state electrolyte. The Br^- substitution for BH_4^- stabilizes the hexagonal structure of $LiBH_4$ at room temperature, whereas Cl^- is soluble only at higher temperatures. Incorporate chloride in hexagonal solid solution lead to increase the energy density of the system. For the first time, a stable hexagonal solid solution of $LiBH_4$ containing both Cl^- and Br- halide anions has been obtained at room temperature (*RT*). The $LiBH_4$-LiBr-LiCl ternary phase diagram has been determined at *RT* by X-ray diffraction coupled with a Rietveld refinement. A solubility of up to 30% of Cl^- in the solid solution has been established. The effect of the halogenation on the Li-ion conductivity and electrochemical stability has been investigated by Electrochemical Impedance Spectroscopy and Cyclic Voltammetry. Considering the ternary samples, h-$Li(BH_4)_{0.7}(Br)_{0.2}(Cl)_{0.1}$ composition showed the highest value for conductivity (1.3×10^{-5} S/cm at 30 °C), which is about three order of magnitude higher than that for pure $LiBH_4$ in the orthorhombic structure. The values of Li-ion conductivity at room temperature depend only on the BH_4^- content in the solid solution, suggesting that the Br/Cl ratio does not affect the defect formation energy in the structure. The chloride anion substitution in the hexagonal structure increases the activation energy, moving from about 0.45 eV for samples without Cl^- ions in the structure, up to about 0.63 eV for h-$Li(BH_4)_{0.6}(Br)_{0.2}(Cl)_{0.2}$ compositions, according with the Meyer-Neldel rule. In addition to increasing Li ion conductivity, the halogenation increase also the thermal stability of the system.

Unlike for the Li-ion conductivity, Br/Cl ratio influences the electrochemical stability: a wide oxidative window of 4.04 V *vs.* Li^+/Li is reached in the Li-Br system, while further addition of Cl is a trade-off between oxidative stability and weight reduction. The halogenation allow both binary and ternary systems operating below 120 °C, thus suggesting possible applications of these fast ion conductors as solid-state electrolyte in Li-ion batteries.

Graphical Abstract

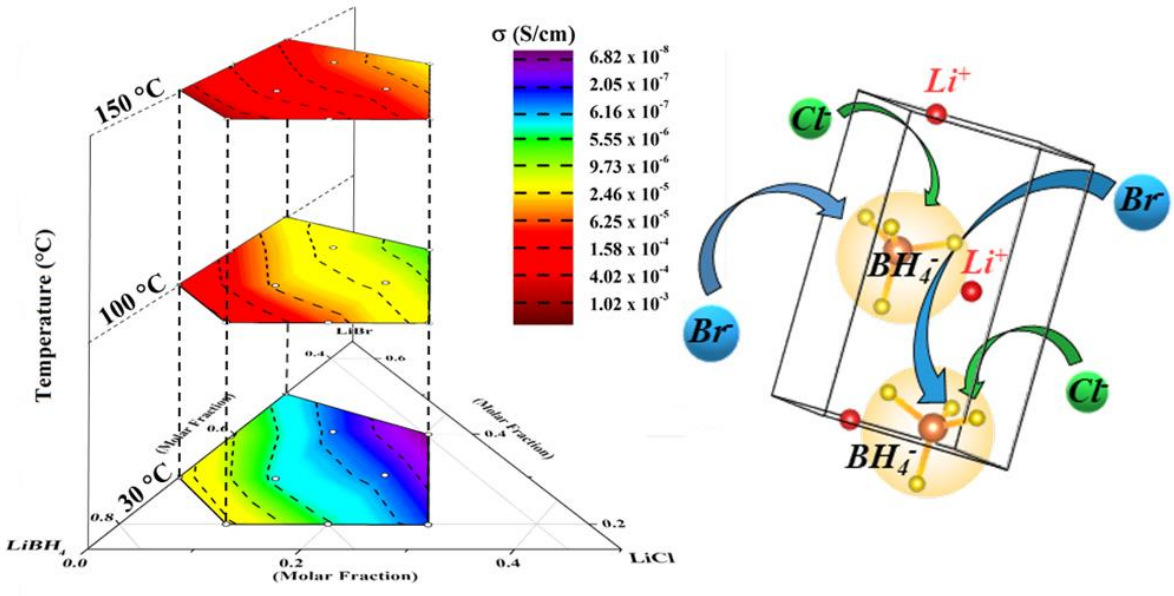

Keywords: complex hydride, solid state electrolyte, Li-ion batteries

1. Introduction

One of the main goals in the current Li-ion battery research is to increase safety and energy density. Nowadays, electrolytes typically consist of lithium salts dissolved in flammable organic solvents, for example in diethyl carbonate (DEC) or tetrahydrofuran (THF).[1] Improved solid electrolytes (SEs) would facilitate the development of a number of emerging technologies, such as all solid-state batteries (SSBs).[2,3] In fact, owing to a very low reduction potential, Li metal is the most desirable anode for high-power applications, but its use in conventional batteries is hampered by the uneven Li plating that results in dangerous shortcuts.[4] SEs could prevent dendrite growth, hence overcoming the risks associated with flammable organic solvents and increasing the life time of the device.[5]

Various types of crystalline solid-state ion conducting materials are known, such as Li_2NH,[6,7] LISICON-type structures,[8] oxides, such as lithium lanthanum titanate (LLTO),[9–12] with a perovskite crystalline structure and NASICON-type structures.[13,14] Recently, also complex hydrides were suggested as solid-state electrolytes.[15–18] $LiBH_4$ is lightweight material (0.666 g/cm^3) and, although used as a strong reducing agent it has a large electrochemical window, being electrochemically stable up to 5 V *vs.* Li^+/Li.[15] It shows a polymorphic transition from an orthorhombic unit cell at room temperature, space group (s.g.) *Pnma*, to an the hexagonal unit cell, s.g. $P6_3mc$,[19] above 110 °C. Despite the hexagonal polymorph having a remarkable ionic conductivity (~10^{-3} S/cm at 120 °C), the orthorhombic low temperature phase is much less conductive with σ amounting to 10^{-8} S/cm at 30 °C making a room temperature (*RT*) battery target unviable.[20]

An essential requirement for a solid-state ion conductor to be used as an electrolyte in a Li-ion battery is a high ionic conductivity at *RT*. Generally speaking, any solid with an ionic conductivity higher than 10^{-3} S/cm and an electronic conductivity lower than 10^{-7} S/cm, can be called as fast ion conductor.[21,22] Ionic conductivity (σ) is an intrinsic property describing charge transport by ion diffusion in the presence of an electric field.[23] The mechanism of ion conduction in solids can be

described as a thermally activated jump of ions in point defect sites (either vacancies or interstitials), which was first described by Frenkel, Schottky and Wagner.[24] The temperature dependence of ionic conductivity (σ) can be described by:

$$\sigma(T) = \frac{\sigma_0}{T} e^{-E_A/k_B T} \quad (1)$$

where E_A is the activation barrier for the jump, σ_0 is an Arrhenius pre-exponential factor, k_B is the Boltzmann constant and T is the temperature. The activation energy (E_A) for ion migration is composed by two terms, $E_A = E_m + E_f/2$,[25–27] where E_m is the migration energy barrier and E_f is the formation energy of the intrinsic defects.

Many studies showed that substitution of BH_4^- anion for halides (e.g. I^- and Br^-) or complex anions (e.g. NH_2^- and NH^{2-}) can either stabilise the hexagonal structure at lower temperatures or promote the formation of new compounds with improved ionic conductivity at *RT*.[15,28–32] Considering the halogenation, the stabilization of the hexagonal solid solution increased the defect formation energy.[33] $LiBH_4$-LiI hexagonal solid solutions showed a high conductivity at *RT*. As an example, a Li-ion conductivity of ~10^{-4} S/cm was measured at 30 °C for a mixture with 25 mol% of LiI.[34] Fast lithium ion conductivity is also retained in $Li(BH_4)_{1-x}Br_x$ ($0.29 \leq x \leq 0.50$) hexagonal solid solutions, although the conductivity is reduced as the bromide content increases above x=0.29.[35] The two complex hydrides, $Li_2(BH_4)(NH_2)$ and $Li_4(BH_4)(NH_2)_3$, exhibit lithium-ion conductivities higher than 10^{-4} S/cm at *RT*.[30,36] Another approach is to increase the ionic conductivity of $LiBH_4$ by mixing it with oxides or by means of nanoconfinement.[37–40]

As described above, halogenation represents a successful strategy to stabilize the $LiBH_4$ conducting phase at *RT*. However, the ionic conductivity alone is not sufficient for designing effective SEs, but it must be flanked by an elevate (electro)chemical compatibility between SE and electrodes. Indeed, conceiving SEs with a large voltage window, allows the use of high-energy positive electrodes, thus increasing the overall amount of energy of the cell,[4] which is nowadays considered the main bottleneck for the development of SSBs.[41]

The aim of this work is to obtain novel solid-state fast ionic conductors based on the hexagonal structure of $LiBH_4$. As described above, halogenation represents a successful strategy to stabilize the $LiBH_4$ conducting phase at *RT*. However, only the heavy Br^- and I^- anions seems to achieve this task, while the use of the lighter Cl^- would be preferred. For this reason, in order to reduce the mass of the electrolyte in solid-state batteries, which is a key parameter to achieve a high energy density, the ternary $LiBH_4$-LiBr-LiCl phase diagram is investigated in this paper and it is discussed herein. An insight on the system is presented, in order to understand phase stability and the solubility limits of the hexagonal solid solution. Once the phase diagram has been defined a complete electrochemical characterization as a function of the halogen content has been performed, in order to assess how halogenations affect the operational voltage window. The combination between structural and electrochemical characterizations provide an efficient tool for screening among the ternary phase diagram the more promising candidates as SE for Li-based SSBs.

2. Experimental

2.1. Synthesis

$LiBH_4$ (purity >95% from Sigma-Aldrich), LiBr (purity >99% from Sigma-Aldrich), LiCl (purity >99% from Merck) and LiI (purity >99% from Sigma-Aldrich) were mixed in different ratios, as reported in **Table 1** and **Figure S1** (Supplementary Information). Before mixing, LiCl and LiBr were dried at 120 °C in a furnace under dynamic vacuum. All manipulations were performed in an argon-filled glovebox (MBraun Lab Star Glove Box supplied with pure 5.5 grade Argon, <1 ppm O_2, <1 ppm H_2O).

Sample Name	Composition (Molar Fraction)		
	$LiBH_4$	**LiBr**	**LiCl**
s1	0.33	0.33	0.33
s2	0.38	0.33	0.29
s3	0.38	0.33	0.29
s4		0.50	0.50
s5	0.80	0.20	
s6	0.70	0.30	

Sample Name	Composition (Molar Fraction)		
s7	0.60	0.40	
s8	0.50	0.50	
s9	0.40	0.60	
s10	0.60	0.20	0.20
s11	0.22	0.58	0.20
s12	0.22	0.19	0.59
s13	0.60	0.10	0.30
s14	0.21	0.69	0.10
s15	0.40	0.50	0.10
s16	0.40	0.40	0.20
s17	0.49	0.41	0.10
s18	0.50	0.30	0.20
s19	0.50	0.20	0.30
s20	0.60	0.30	0.10
s21	0.70	0.20	0.10

Table 1. *Composition of the investigated samples.*

An equimolar mixture of LiBr and LiCl (sample ***s4***) was prepared to verify the Vegard's law in the LiBr-LiCl binary system[42] (see Supplementary Information). To confirm the miscibility range of $(LiBH_4)_{1-x}(LiBr)_x$, a batch of binary samples were prepared in the $0.4<x<0.8$ composition range (samples ***s5-s9***).

A Fritsch Pulverisette 6 planetary mill was used to ball mill the reactants under argon atmosphere in 80 mL tungsten carbide vials, with tungsten carbide balls (10 mm o.d.) and a balls-to-sample mass ratio of 30:1. In order to optimize the synthesis conditions, the sample ***s3*** was milled for different times. All mixtures were then ball milled (BM) for 1,5 hours at 350 r.p.m., in periods of 10 min separated by 2 min breaks, to minimize possible heating effects (see Supporting Information). In order to reach the equilibrium conditions, all samples were annealed (AN) at 250 °C for 2 or 4 h (**Figure S1**) in a quartz tube under static vacuum, with a heating/cooling rate of 5 °C/min.

2.2. Characterization

2.2.1. X-ray Powder Diffraction (XPD)

The as-milled and annealed powders, were characterised by XPD at *RT* using a Panalytical X-pert Pro MPD (Cu $K_{\alpha1}$ = 1.54059 Å, $K_{\alpha2}$ = 1.54446 Å) in Debye-Scherer geometry. Patterns were collected from 10° to 70° 2θ range, with a step size 0.016, a time step of 60 s for a total of 30 min per scan. 0.5 mm glass capillaries were filled with the sample powder and sealed under Ar atmosphere. The Rietveld refinement of diffraction patterns has been performed using the MAUD (Materials Analysis Using Diffraction) software,[43] considering Rwp and χ as indicators for the quality of the fitting.

2.2.2. Attenuated Total Reflectance Infrared Spectroscopy (ATR-IR)

Infrared spectra were collected in Attenuated Total Reflection mode with a Bruker Alpha-P spectrometer, equipped with a diamond crystal. The instrument was placed inside a nitrogen filled glove-box. All spectra were recorded in the 5000− 400 cm^{-1} range with a resolution of 2 cm^{-1}. Reported data are an average of 64 scans.

2.2.3. High-Pressure Differential Scanning Calorimetry (HP-DSC)

A 204 Netzsch HP-DSC was used to analyze the thermal stability of the samples, avoiding decomposition and obtaining accurate value of phase transformations temperature and enthalpies. The calorimeter was placed inside an Ar filled glove box, to ensure sample handling under inert atmosphere. Approximately 5–10 mg of sample was loaded into closed aluminium crucibles with a lid. Samples were heated and cooled in the desired temperature range at 5 °C/min under 10 bar of H_2.

2.2.4. Electrochemical Impedance Spectroscopy (EIS)

The Li-ion conductivity was measured by means of EIS using a HP4192A LF impedance analyser (frequency range 5 Hz ÷ 2 MHz, applied voltage 10 mV) and a Novocontrol sample cell BDS 1200. Samples were compacted into pellets (diameter 10 mm, thickness 0.2-0.6 mm) with an axial hydraulic press at about 60 MPa. Gold disks were used as blocking electrodes. EIS was performed every 10 °C in the temperature range $RT < T < 150$ °C. Two cycles were performed and analysed

for selected samples in order to verify the reproducibility of the measurements. Impedance data were analysed via the EqC software,[44] following the data validation described in ref.[45] All fits performed resulted in $\chi^2 < 10^{-3}$.

2.2.5 Cyclic Voltammetry (CV)

The electrochemical stability was measured by means of CV. The samples were prepared by mixing the desired compound with the carbon black (CB, Ketjenblack EC600JD, Akzo Nobel Chemicals) into an agate mortar (20:1 weight ratio). Then a two layer pellet was created with 8 mg of such mix and 25 mg of the pure compound, by cold pressing into an axial hydraulic press, at 240 MPa (diameter 6 mm). The obtained pellets were therefore tested in a 2-electrode ¾" PTFE Swagelok-type cell, with a lithium disk as counter and reference electrode and with a gold disk as current collector, in contact with the sample+CB side of the pellet. The cells were tested into a Biologic MPG-2 after 24 hour rest at the desired temperature. CV measurements have been performed into a voltage region -1<V<5 V vs. Li^+/Li, at a scanning rate of 0.5 mV/s.

3. Results and discussion

3.1 Structural characterization

Figure 1a shows XPD patterns of a $LiBH_4$-LiBr-LiCl equimolar mixture (sample ***s1***) after BM (bottom) and after AN (top). After ball milling (BM), the high temperature hexagonal phase of $LiBH_4$ is already stabilized at *RT*, but main diffraction peaks of the orthorhombic phase, stable at *RT,* are still present in the pattern**.**

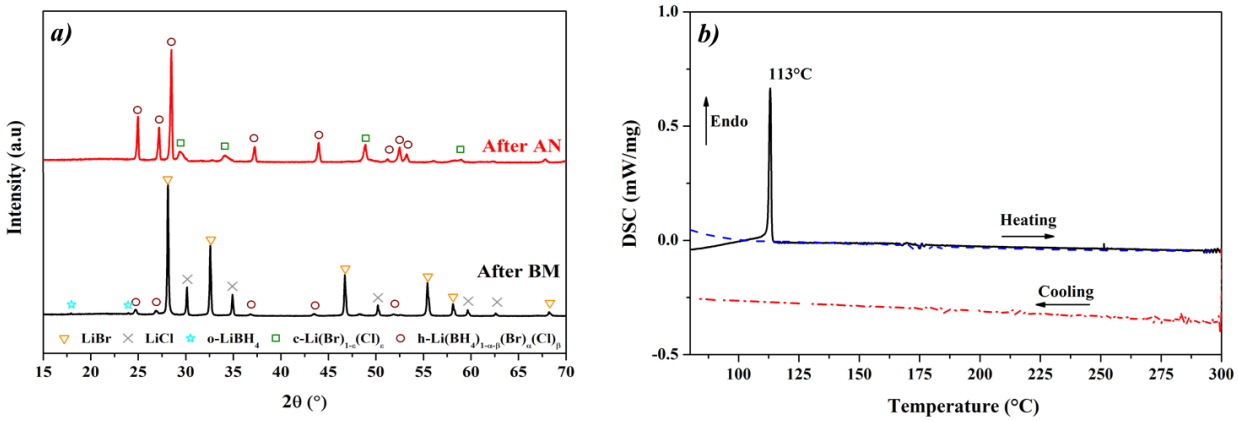

Figure 1. *(a) X-ray diffraction patterns of sample* ***s1*** *after ball milling (bottom) and after annealing (top). (b) HP-DSC trace of sample* ***s1*** *after ball milling. The solid and dash-dot lines show the results of the first heating and cooling ramps, respectively, while the dash line refers to the second heating ramp.*

The relative amount of the hexagonal phase cannot be directly determined by Rietveld analysis at this stage, since its composition is unknown. Nevertheless, it is hereby confirmed that a mechanochemical treatment of the $LiBH_4$-LiBr-LiCl system allows the stabilization of the high temperature hexagonal phase at *RT*. However, the presence of XPD peaks related to LiBr and LiCl $Fm\bar{3}m$ cubic phase (a = 5.50 Å and a = 5.14 Å, respectively) denotes an incomplete solubilisation of halide anions.

The calorimetric analysis of the sample ***s1*** after BM (**Figure 1b**) shows an endothermic peak due to the phase transition of $LiBH_4$ at 113 °C (peak temperature), confirming the presence of residual orthorhombic $LiBH_4$ in the ball milled mixture. The peak integration provides an enthalpy of transition of 1.5 kJ/mol. This value corresponds to about 28% of the tabulated value (5.3 kJ/mol),[46] indicating that most of $LiBH_4$ is already in the hexagonal phase after BM. The observed phase transition is irreversible, suggesting that a heating up to 300 °C is suitable to promote the complete stabilization of $LiBH_4$ in the hexagonal phase as solid solution. In fact, XPD performed after AN (**Figure 1a**), does not show any diffraction peak related to the orthorhombic phase.

Bragg peaks of the hexagonal solid solution after AN are shifted to higher 2θ values compared those observed after BM (**Figure 1a**), suggesting a contraction of the unit cell.

In the XPD pattern obtained after AN, a cubic phase corresponding to the $Li(Br)_{1-\varepsilon}(Cl)_{\varepsilon}$ cubic solid solution is still present, with a lattice parameter (a = 5.25 Å) lying between those of pure LiCl and LiBr compounds. Having verified that Vegard's law holds for such system (see **Figure S2** in Supporting Information), the composition of the cubic solid solution resulting from the value of the lattice parameter corresponds to $LiBr_{0.28}Cl_{0.72}$.

In order to calculate the composition of the hexagonal solid solution in the mixture, the following molar balance has been solved:

$$f \times Li[\alpha Br \cdot \beta Cl \cdot (1-\alpha-\beta)BH_4] + (1-f) \times Li[\varepsilon Cl \cdot (1-\varepsilon)Br] = 1 \qquad (2)$$

where f and $(1-f)$ are the molar fractions of the hexagonal solid solution $Li(BH_4)_{1-\alpha-\beta}(Br)_{\alpha}(Cl)_{\beta}$ and of the cubic solid solution $Li(Br)_{1-\varepsilon}(Cl)_{\varepsilon}$, respectively; α, β and $(1-\alpha-\beta)$ are the molar fractions in the hexagonal structure, i.e. occupancy, of Br^-, Cl^- and BH_4^- anions, while ε and $(1-\varepsilon)$ refers to molar fraction of Br^- and Cl^- in the cubic structure of the $Li(Br)_{1-\varepsilon}(Cl)_{\varepsilon}$ solid solution. Equation (2) is not solvable with a linear method. In order to overcome this problem, a self-consistent iterative method has been applied. To start with, the occupancy of Cl^- (β) in the hexagonal structure has been taken equal to 0.2 and the composition of $Li(Br)_{1-\varepsilon}(Cl)_{\varepsilon}$ cubic solid solution, calculated from the lattice parameter as mentioned above, has been fixed (i.e. ε = 0.72). In this way, the equation $f \times \alpha + (1-f) \times 0.28 = f \times \beta + (1-f) \times 0.72 = 0.33$ has been solved to obtain a starting value for the occupancy of Br^- (α) in the hexagonal structure. The estimated compositions of both phases (i.e. α, β and ε values) have been used as starting parameters for performing the Rietveld refinement.

For the Rietveld refinement of the XPD patterns, the structural model of the hexagonal polymorph of $LiBH_4$ ($P6_3mc$) was used to describe the structure of h-$Li(BH_4)_{1-\alpha-\beta}(Br)_{\alpha}(Cl)_{\beta}$ solid solution, where Br^- and Cl^- ions were constrained to lie on the same boron position (2*b* Wyckoff site). The

value of the molar fraction (f) obtained from the refinement has been then used in equation (2) to obtain a new starting value for α. The process has been repeated recursively until a convergence was reached, leading to a relative phase fraction and compositions corresponding to 14 wt.% of c-$LiBr_{0.28}Cl_{0.72}$ solid solution and 86 wt.% of h-$Li(BH_4)_{0.39}Br_{0.33}Cl_{0.28}$ (**Figure S3**).

The lattice parameters of the hexagonal phase, obtained from the Rietveld refinement of the XPD pattern after AN, are a = 4.12 Å and c = 6.57 Å, corresponding to a cell volume equal to 96 $Å^3$ .The value of cell volume of pure h-$LiBH_4$ at *RT* has been evaluated equal to 106 $Å^3$, using the experimental value of 114 $Å^3$ obtained at 262 °C,[47] and a volumetric thermal expansion coefficient of 2.9×10^{-4} K^{-1}.[47] A contraction of the cell volume of the hexagonal solid solution is expected after halogenation, due to the smaller ionic radii of Cl^- ($r(Cl^-)$ = 1.81 Å) and Br^- ($r(Br^-)$ = 1.96 Å)[48] compared to that of BH_4^- ($r(BH_4^-)$ = 2.03 Å)[49–51]. So, from the observed cell volume contraction of about 9%, a successful halogenation in the hexagonal solid solution is confirmed for the AN sample.

On the basis of the calculated compositions of the hexagonal solid solution in sample ***s1***, a $(LiBH_4)_{0.39}(LiBr)_{0.33}(LiCl)_{0.28}$ (sample ***s2***) mixture has been synthetized to obtain a single phase hexagonal solid solution. **Figure 2a** shows the XPD diffraction patterns of the BM and AN samples. The result of the Rietveld refinement of AN sample is shown in **Figure 2b**. In the pattern of sample after BM, diffraction peaks of o-$LiBH_4$ are not present, indicating that all $LiBH_4$ is in the hexagonal phase. In fact, in the HP-DSC trace of sample BM, the endothermic peak due to the phase transition of $LiBH_4$ is not present, confirming that all $LiBH_4$ is in the hexagonal phase after the mechanical treatment (**Figure S4**).

As evidenced in the XPD pattern of ***s2*** sample AN (**Figure 2b**), the estimated limit of solubility for the ternary solid solution is confirmed by the presence of a basically single hexagonal phase (i.e. only 2 wt.% of $LiBr_{0.38}Cl_{0.62}$ is still present). For the first time, a single hexagonal solid solution of

h-$LiBH_4$ containing two different halide anions (Br^- and Cl^-) has been obtained at *RT*. The stability of the solid solution was evaluated over time, i.e. after about one-year, at *RT* and a very similar X-ray diffraction pattern was obtained for the sample ***s2***, indicating long-term stability of the solid solution (**Figure S5**).

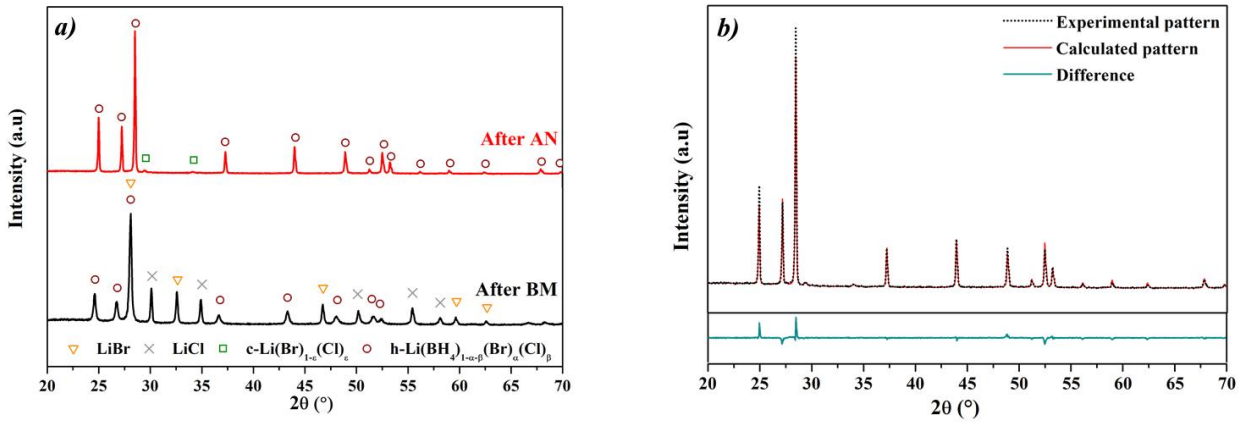

Figure 2. *a) X-ray diffraction patterns of $(LiBH_4)_{0.39}(LiBr)_{0.33}(LiCl)_{0.28}$ mixture (sample **s2**) after ball milling (bottom) and after annealing (top). b) Results of the Rietveld refinement of sample **s2** after AN (Rwp=8.34 %, χ=1.65).*

In order to study the changes in the vibrational properties of lithium borohydride, due to the stabilization of the hexagonal phase by halide additions, IR-ATR spectroscopy was performed on AN sample ***s2*** and the result is shown in **Figure 3**, together with the spectrum for pure o-$LiBH_4$. In fact, changes in the IR-ATR spectrum reflect a change in the site symmetry of the BH_4^- anions, due to the formation of a solid solution.

The isolated BH_4^- anion has an ideal tetrahedral symmetry, T_d. However, the vibrational modes are split in the crystalline state due to lowering of the site symmetry from T_d to C_s, *i.e.* the degenerate fundamental modes $\tilde{\nu}_2$, $\tilde{\nu}_3$, and $\tilde{\nu}_4$ split into several components.[52,53] The IR-ATR spectrum of as-received o-$LiBH_4$ shows two main sets of IR absorption bands, due to B–H stretching (2400–2000 cm^{-1} region) and B–H bending (1600–800 cm^{-1} region) vibrational modes, as reported in the

literature.[52,54–57] In h-$LiBH_4$ structure, the BH_4^- anions have C_{3v} site symmetry and $\tilde{\nu}_3$ has only two components, while the mode $\tilde{\nu}_2$ is doubly degenerate.[52] Therefore, the changes in the spectrum of hexagonal solid solution could be related to the change of BH_4^- site symmetry.

The IR-ATR spectrum of sample **s2** after AN shows differences in the BH_4^- bending and stretching regions with respect to the spectrum of o-$LiBH_4$, i.e. a decrease of the number of the components related to $\tilde{\nu}_2$ and $\tilde{\nu}_3$ fundamental modes (**Figure 3**). A similar behaviour has been observed by Rude et al. for the hexagonal phase of $LiBH_4$ stabilized at *RT* by Br^-[52] and I^-[57] substitutions. Furthermore, new peaks are present at ~1170 cm^{-1}, 1020 and 958 cm^{-1}, indicating a slight shift of the fundamental modes of BH_4^- owing to the presence of Br^- and Cl^- anions, according to the literature.[52,57] Finally, it is worth noting that pure halides vibrational modes cannot be observed in the investigated spectral range.

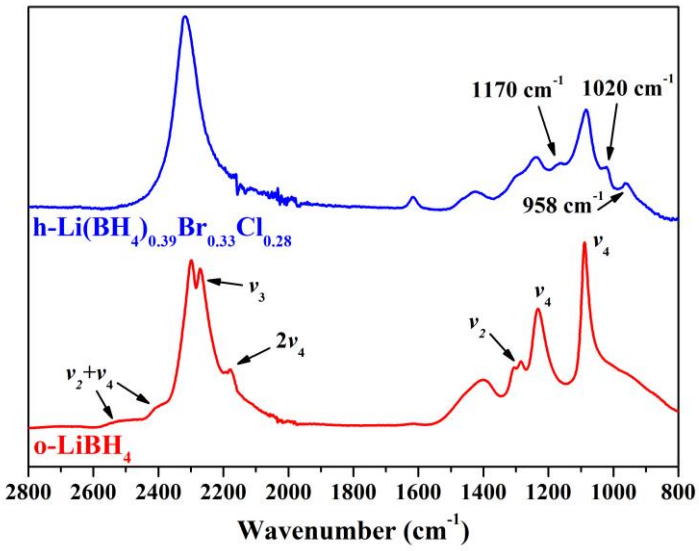

Figure 3. *IR-ATR spectrum of pure $LiBH_4$ (bottom) and sample **s2** after AN (top). IR active modes are indicated in the figure and described in the text.*

Usually, both mechanical and thermal treatments are necessary to obtain a single lithium borohydride-halide hexagonal solid solution.[52,57,58] However, after 24 h of milling, a complete solid solution h-$Li(BH_4)_{0.667}Br_{0.333}$ was successfully obtained by Sveinbjörnsson et al.[35] In order to

investigate the feasibility to form a 3-anions hexagonal phase only by mechanochemistry, the same composition of the sample ***s2*** was ball milled for different times (sample ***s3***). **Figure S6** shows the effect of the increasing milling time on the formation of the hexagonal solid solution. After 1 h of milling, the hexagonal solid solution is already formed, as observed for sample ***s2***. Upon further milling, the progressive dissolution of LiBr and LiCl into h-$LiBH_4$ is observed, as evidenced by a gradual intensity decrease of Bragg peaks of halide phases. The mechanochemical treatment alone failed to promote the complete solubility of both Br^- and Cl^- halide anions in the hexagonal solid solution. In fact, even after 41 h of ball milling, residual $Li(Br)_{1-\varepsilon}(Cl)_\varepsilon$ is still present, which disappears after annealing (**Figure S6**).

A small difference in ionic radius is promoting the formation of solid solutions.[59] Indeed, for $LiBH_4$-LiI and $LiBH_4$-LiBr systems, that have similar anionic radii, a significant miscibility is expected and confirmed experimentally, with the stability of the hexagonal phase at *RT*.[32,35,52,57] On the other hand, Cl^- anion is miscible in h-$LiBH_4$ only at temperatures close to 100 °C.[60] In fact, the radii of BH_4^- and Cl^- differ significantly. It can therefore be concluded that the presence of Br^- in the solid solution promotes the Cl^- solubilisation.

The occurrence of a negative enthalpy of mixing (ΔH_{mix}) promotes the formation of a solid solution, as in the case of $LiBH_4$-LiI and $LiBH_4$-LiBr systems.[52,57] In addition, from ab-initio calculations, a negative ΔH_{mix} has been also estimated for the $LiBH_4$-LiCl hexagonal solid solution,[60] however insufficient to stabilize the hexagonal solid solution at *RT*. On the other hands, the entropy of mixing (ΔS_{mix}) in a solid solution increases with the number of different anions. As a consequence, a more negative free energy of mixing ($\Delta G_{mix}=\Delta H_{mix}-T\Delta S_{mix}$) is expected in the hexagonal solid solution for the $LiBH_4$-LiBr-LiCl system with respect to the binaries, making it stable at *RT*.

3.2 Solubility limits in the $LiBH_4$-LiCl-LiBr system

In order to have an optimized control of the synthesis process and to obtain single phase samples, the solubility limits at *RT* of the hexagonal solid solution in the $LiBH_4$-LiCl-LiBr system have been

investigated. Several samples prepared by BM + AN (**Table 1** and **Figure S1**) have been analysed by XPD, determining the phase amount and compositions by Rietveld refinement, following the procedure described above. By solving equation (2) (see paragraph 3.1) the solubility limits of the hexagonal solid solution were defined. The calculated mutual molar quantity of phases has been checked with respect to the level rule,[61] confirming the reliability of calculations.

The solubility limits in the $LiBH_4$-LiBr system were determined by Sveinbjörnsson et al.[35] and confirmed in this study (samples ***s5-s9***). The $Li(BH_4)_{1-\alpha}(Br)_\alpha$ hexagonal solid solution is stable at *RT* as a single phase from α = 0.3 to α = 0.5. For concentrations α > 0.5, the hexagonal solid solution coexists with cubic LiBr (sample ***s9***). For the sample ***s9***, the lattice parameter of LiBr was refined as a_{LiBr} = 5.50 Å, which turns out equal to that of the pure compound, indicating no solubility of BH_4^- in the cubic structure of LiBr. Therefore, a positive heat of mixing is expected for the corresponding solid solution. For α < 0.3, an orthorhombic o-$Li(BH_4)_{1-\alpha}Br_\alpha$ phase is present together with the hexagonal solid solution, with lower cell parameters with respect to those of pure o-$LiBH_4$, in agreement with Sveinbjörnsson et al.,[35] who observed a single orthorhombic phase for α < 0.1.

In order to define the solubility limits in the hexagonal $Li(BH_4)_{1-\alpha-\beta}(Br)_\alpha(Cl)_\beta$ solid solution, samples ***s10-s14*** were prepared. All samples are biphasic, containing both hexagonal and halide cubic solid solutions, with the exception of $(LiBH_4)_{0.6}(LiBr)_{0.2}(LiCl)_{0.2}$ (sample ***s10***), which shows a single hexagonal phase. In order to explore in details the hexagonal solid solution, the monophasic zone was mapped with seven different samples (sample ***s15-s21***), in which a single hexagonal phase was observed.

The maximum chloride concentration obtained in the h-$Li(BH_4)_{1-\alpha-\beta}(Br)_\alpha(Cl)_\beta$ solid solution amount to β = 0.31 in sample ***s13***, where h-$Li(BH_4)_{0.45}(Br)_{0.24}(Cl)_{0.31}$ phase coexists with the cubic solid solution c-$Li(Br)_{0.17}(Cl)_{0.83}$. $(LiBH_4)_{0.6}(LiBr)_{0.1}(LiCl)_{0.3}$ (sample ***s13***) contains pure LiCl and the hexagonal solid solution h-$Li(BH_4)_{0.62}(Br)_{0.1}(Cl)_{0.28}$, representing the limit of the biphasic zone.

Figure 4 shows the obtained ternary phase diagram at *RT*. The diagram is composed by: (*a*) hexagonal h-$Li(BH_4)_{1-\alpha-\beta}(Br)_\alpha(Cl)_\beta$ monophasic zone; (*b*) cubic c-$Li(Br)_{1-\varepsilon}(Cl)_\varepsilon$ monophasic zone (on LiBr-LiCl axis); (*c*) orthorhombic o-$Li(BH_4)_{1-\alpha}(Br)_\alpha$ monophasic zone (on $LiBH_4$-LiBr axis); (*d*) biphasic zone (*Cub+Hex*), in which are present h-$Li(BH_4)_{1-\alpha-\beta}(Br)_\alpha(Cl)_\beta$ in equilibrium with c-$Li(Cl)_{1-\varepsilon}(Br)_\varepsilon$; (*e*) biphasic zone (*Hex+Ort*), where h-$Li(BH_4)_{1-\alpha-\beta}(Br)_\alpha(Cl)_\beta$ and the orthorhombic solid solution (o-$Li(BH_4)_{0.9}Br_{0.1}$) are present; (*f*) biphasic zone (*LiCl+Ort*), containing o-$Li(BH_4)_{1-\alpha}Br_\alpha$ and LiCl; (*g*) triphasic zone, where h-$Li(BH_4)_{0.62}(Br)_{0.1}(Cl)_{0.28}$, o-$Li(BH_4)_{1-\alpha}Br_\alpha$ and pure LiCl phases are in equilibrium.

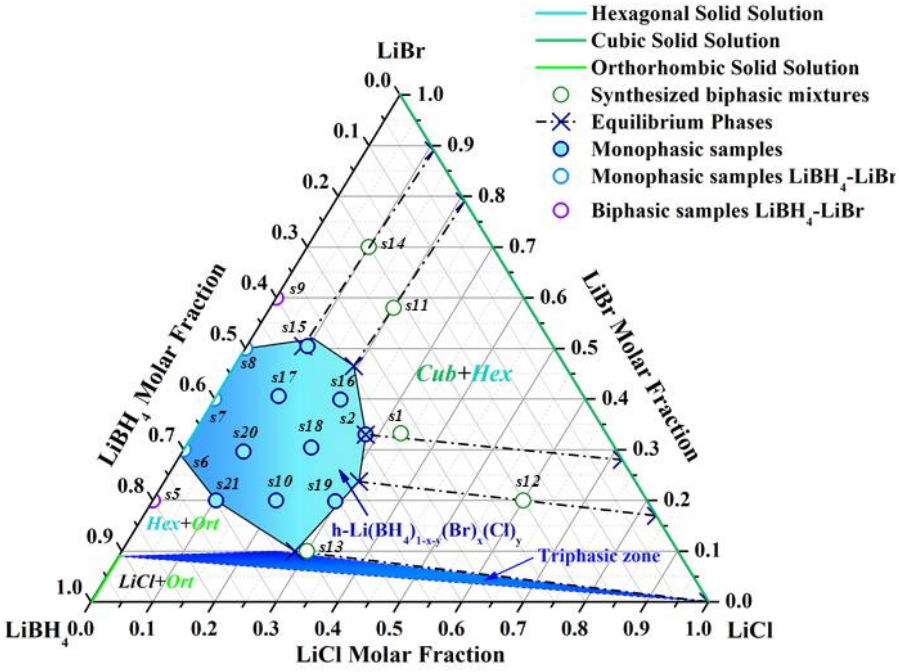

Figure 4. *Ternary phase diagram of $LiBH_4$-LiBr-LiCl system at room temperature, obtained by X-ray diffraction analysis. Light filled area is the monophasic zone of hexagonal $Li(BH_4)_{1-\alpha-\beta}(Br)_\alpha(Cl)_\beta$ solid solution. Dark filled area indicates a triphasic zone, where $Li(BH_4)_{0.62}(Br)_{0.1}(Cl)_{0.28}$, o-$Li(BH_4)_{0.9}Br_{0.1}$ and pure LiCl are present. The analysed samples are indicated in the figure and they refer to Table 1.*

Since the unit cell volume is expected to affect the Li-ion conductivity, as observed in different systems,[58,62,63] lattice parameters of h-$Li(BH_4)_{1-\alpha-\beta}(Br)_\alpha(Cl)_\beta$ solid solutions were determined from

the Rietveld refinement. In order to highlight the effect of composition, the values of lattice constants and volume obtained for sample ***s6*** have been taken as a reference and data are reported as relative variations. **Figure 5**, shows that both *a* and *c* lattice constants, as well as the volume, of the hexagonal solid solution decrease with increasing of the concentration of both halides, as discussed above. The contraction of lattice parameters is nearly linear with increasing Cl^- concentration. When Br^- replaces the borohydride anions, the decrease of lattice parameters and volume is less pronounced with respect to Cl^-.

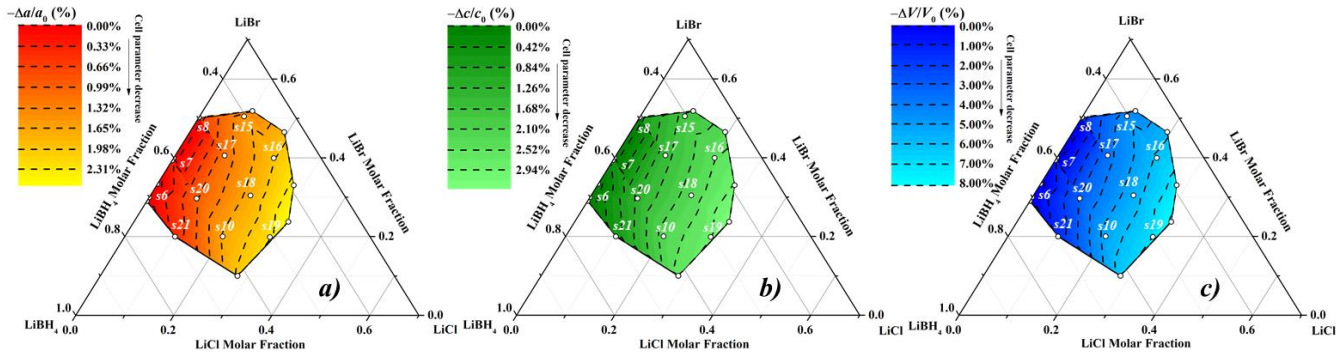

Figure 5. *RT maps of (a) –(Δa)/a_0 % cell parameter (b) –(Δc)/c_0 % c cell parameter and (c) –(ΔV)/V_0 % volume of the hexagonal solid solution h-Li$(BH_4)_{1-\alpha-\beta}(Br)_\alpha(Cl)_\beta$ obtained by Rietveld refinement. a_0, c_0 and V_0 refer to the parameters of sample* ***s6*** *taken as a reference. Δ represents the variation of the cell parameters and volume with respect to the reference values. Dashed lines correspond of the values and lines shown in the legend.*

3.3 Li-ion conductivity

In order to investigate the trend of Li-ion conductivity as a function of composition and temperature, temperature-dependent EIS measurements were performed in the temperature range 30 < *T* < 150 °C for samples showing a single hexagonal phase in order to investigate the trend of Li-ion conductivity as a function of composition and temperature.

As an example, data obtained for sample ***s20*** are reported in **Figure 6**. The impedance spectrum is composed, close to room temperature (30 °C), by a single arc in the Nyquist plot (**Figure 6a**), while, at a higher temperature (110 °C), an additional linear dispersion is visible in the low frequency region (**Figure 6b**). A constant phase element ($CPE_{Electrodes}$) was used to describe the non-ideal diffusion between the blocking electrodes.[64] The ideality factor was in any case α>0.9. The bulk property was modelled with a CPE_{Bulk} in parallel with a resistor, representing the Li^+ diffusion.

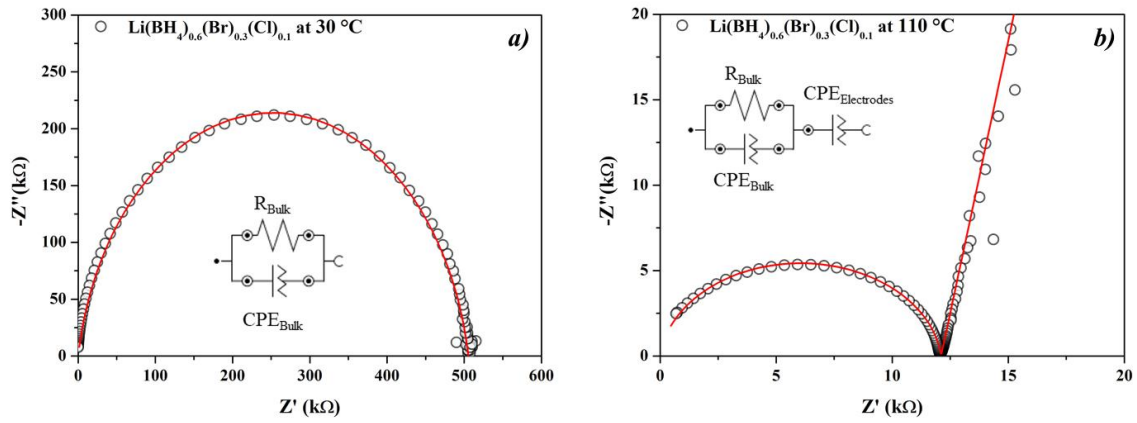

Figure 6. *Impedance spectra shown on the Nyquist plot for the sample* ***s20*** *collected at (a) 30 °C and (b) 110 °C. The insets show the equivalent electrical circuits used to fit the data.*

The equivalent electrical circuits used to fit the impedance data are shown in the insets of **Figure 6**. The second component describes the electrolyte/electrode interface, while the first takes into account the bulk conductivity. It is not possible to separate the single arc in more than one contribution (as in the case of grain boundary and bulk diffusion), even if the shape of the single arc would suggest the contrary. At high temperatures (*i.e.* above 120 °C), where the bulk arc cannot be resolved due to the setup limitation, the resistance was determined by the intercept on the real axis of the prolongation of the $CPE_{Electrodes}$ response.

The Li-ion conductivity of the samples was calculated according to:

$$\sigma = \frac{d}{AR} \tag{3}$$

where *R* is the resistance obtained from the fit of EIS data, *d* is the thickness of the sample, and *A* is its area. Results of Li-ion conductivity obtained for different compositions of the hexagonal solid solution (samples ***s6***, ***s7***, ***s8***, ***s10***, ***s16***, ***s17***, ***s18***, ***s19***, ***s20***, and ***s21***) as a function of inverse temperature are reported in **Figure 7a**. An overview of data as function of temperature and composition is shown in **Figure 7b.**

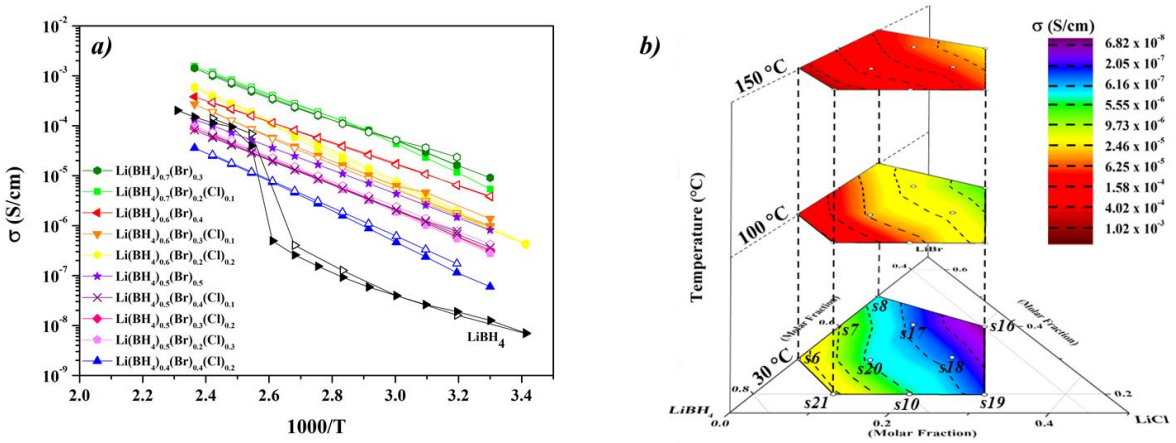

Figure 7. *(a) Li-ion conductivity of samples in the hexagonal solid solution in the $LiBH_4$-LiBr-LiCl system. Open symbols represent the cooling ramp, close symbols the heating one. b) Contour map of Li-ion conductivity as a function of composition for three selected temperatures. Iso-conductivity dashed lines correspond to the values and lines shown in the legend.*

As expected, for single-phase samples containing the hexagonal solid solution, the change in the conductivity due to the polymorphic transition, as observed for pure $LiBH_4$, disappears. h-$Li(BH_4)_{0.7}(Br)_{0.2}(Cl)_{0.1}$ (sample ***s21***) shows the highest value for conductivity (1.3×10^{-5} S/cm at 30 °C) inside the ternary solid solution range. It is worth noting that this value is three orders of magnitude higher than that of pure $LiBH_4$ at *RT*. In any cases, considering also the binary solid solution, $Li(BH_4)_{0.7}(Br)_{0.3}$ (sample **s6**) shows the highest value for Li-ion conductivity at *RT*. As

shown in **Figure 7,** the conductivity values for several compositions in the solid solution range are greater than that of pure hexagonal $LiBH_4$, in the same temperature range.

As shown in **Figure 7**, the conductivity increases with temperature, as expected for a thermally activated process. Plots of $\ln(\sigma T)$ as a function of 1000/T show a linear trend, in agreement with equation (1). So, the activation energy (E_A) for Li-ion conductivity was obtained by a linear fit of the Arrhenius plot and the results are shown as a function of composition in **Figure 8**. The lowest values of activation energy are observed for the $LiBH_4$-LiBr solid solutions (e.g. 0.45 eV for sample ***s7***).

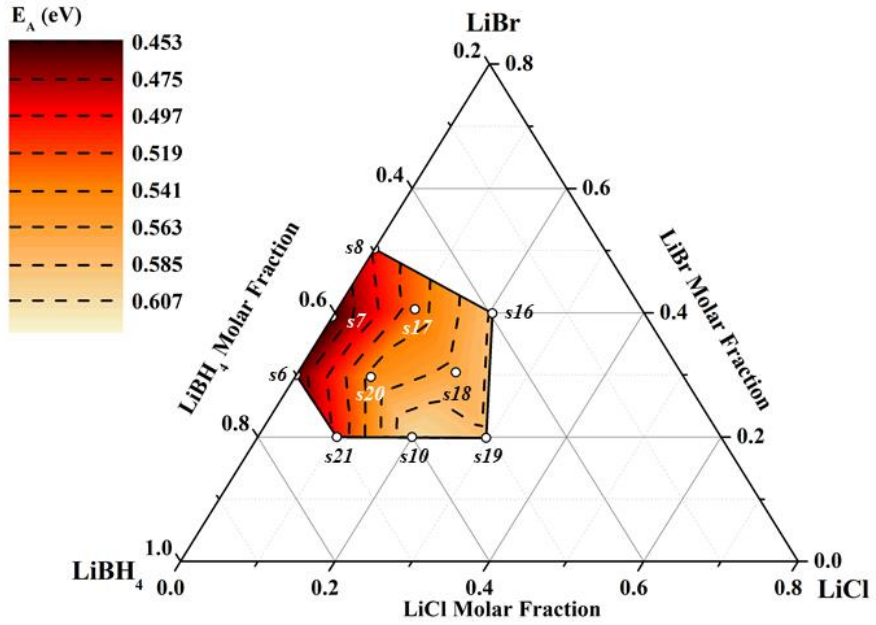

Figure 8. *Contour map of activation energy for Li-ion conductivity for samples in the hexagonal solid solution in the $LiBH_4$-LiBr-LiCl system as a function of composition. Iso-activation energy dashed lines correspond of the values and lines shown in the legend.*

Collected data show that a correlation exists between composition and ionic transport properties, as represented by the Li-ion conductivity and activation energy. Decreasing the BH_4^- content in the hexagonal solid solution, the Li-ion conductivity of the sample decreases, meaning that the presence of BH_4^- anions in the structure promotes the Li-ion mobility. The **Figure 7** also shows that, the

conductivity does not dependent on Br^-/Cl^- ratio. In fact, in the hexagonal structure, BH_4^- possess rapid reorientation,[65,66] so that the rotational freedom of the BH_4^- could have positive effects on the Li^+ conductivity. The dependence of Li ion conductivity as a function of the BH_4^- content reported here is in good agreement with the calculations reported by Yao et al.[33], where by density functional theory (DFT) calculations has been highlighted that increase of the halide concentration in the solid solution increases the formation energy for Li defect (vacancies, interstitials and Frenkel couples), reducing the Li defect concentration. In addition, considering In $Li(BH_4)_{1-x}I_x$, solid solution, higher I^- concentration yielded a higher diffusivity but with a lower conductivity,[33] according with our results, where increasing the halide concentration causes a decreasing of the Li-ion conductivity.

It is worth noting that, increasing the Cl^- content in the hexagonal solid solution, the density of the electrolyte decreases, as shown in **Figure S7**, where the calculated density of the hexagonal solid solution is reported as a function of composition. The density of the h-$Li(BH_4)_{0.7}(Br)_{0.2}(Cl)_{0.1}$ (sample ***s21***) and h-$Li(BH_4)_{0.7}(Br)_{0.3}$ (sample ***s6***) is 1.19 and 1.32 g/cm^3, respectively, but the Li-ion conductivity is almost the same (**Figure 7**). So, the addition of Cl^- in the hexagonal solid solution leads to lighter ion conductors with similar conductivity, suggesting possible applications of these fast ion conductors as electrolytes to increase the energy density in Li-ion solid-state batteries.

The activation energy does not dependent on BH_4^-/Br^- ratio (**Figure 8**), but it increases with increasing the content of Cl^- in the hexagonal solid solution, reaching values higher than 0.6 eV (e.g. 0.63 eV for sample ***s10***). It is clear that the addition of Cl^- in the h-$Li(BH_4)_{1-x}(Br)_x(Cl)_y$ phase increases the activation energy for the Li-ion jump, without affecting significantly the Li-ion conductivity. The values of cell volume and activation energy correlates, suggesting that the latter is controlled by the former. This observation is confirmed in **Figure S8**, which shows that the activation energy decreases as a function of the cell volume.

As shown previously, the dissolution of Cl^- anion in the hexagonal structure decreases the cell volume, does not affect significantly the ionic conductivity, but increases the activation energy. Using conventional hopping theory,[67] the pre-exponential factor σ_0 can be defined as:

$$\sigma_0 = \frac{zn(Ze)^2}{k_B}\exp(\frac{\Delta S_m}{k_B})a_0^2 v_0 \quad (4)$$

where z is a geometrical factor, which takes into account different diffusion geometries and correlation factors, Ze is the charge of the ion, n is the carrier density of mobile ions, ΔS_m is the migration entropy, a_0 is the jump distance and v_0 is the jump frequency. In the case of ionic conductors, the substitution with more polarizable anions in the sublattice causes a softening of the lattice.[62,63] This leads to a lower oscillation frequency of the moving cation, that decreases both the migration entropy and enthalpy (*i.e.* the activation energy).[62,63] This is clearly valid in $Li(BH_4)$-LiX systems (where X = Br and I) since the polarizability of BH_4^- results bigger than Cl^- (3.90 and 2.96 $Å^3$, respectively) but smaller than Br- and I- (4.16 and 6.43 $Å^3$, respectively).[68]

In order to elucidate the relation between anions polarizability and conduction mechanism in the hexagonal solid solution, the Mayer-Neldel plot (M-N) was built, plotting the natural logarithm of the pre-exponential factor, σ_0, against the activation energy E_A (**Figure 9**).

The M-N rule is an empirical law that describes a group of physical properties that are Arrhenius-like dependent,[69] recently analysed to show the interplay between ionic conductivity and lattice rigidity in different compounds as argyrodites and LGPS thiophosphates.[62,70,71] According to Yelon et al.[72], in the M-N plot the stiffer the lattice, the flatter the slope. Hence, from **Figure 9**, three regions can be defined, corresponding to three different degrees of lattice stiffness, according to the amount of BH_4^- in the structure.

The phonon spectra of $LiBH_4$ was exhaustively investigated by Gremaud et al.[73] and consequently many efforts were focused on the understanding of BH_4^- dynamics, therefore investigating a different spectral phonon region (i.e. librations, bending and stretching modes). The crystal

stiffness, however, is directly related to the acoustic branch of the normal modes. We are not aware, up to our knowledge of any study, on the phonon spectra modification of $LiBH_4$ by halogenation. Even if it is impossible to quantify this aspect, a stiffer lattice was shown to be preferable in terms of Li^+ mobility (at least for thiophosphates)[70] which would suggest to point at Cl^- as preferred candidate to achieve the optimal configuration.

When the borohydride is replaced by the halide, the lattice rigidity increases, according to the modification of the phonon spectra and the suppression of the normal modes proper of the BH_4 tetrahedra. According to **Figure 9**, the edge between *soft* and *hard* hexagonal lattice can lie between $0.5 < BH_4 < 0.6$ per formula unit. On the other hand, **Figure 8** and **9** clearly show that, once the BH_4 content is fixed, the activation energy scales up with the amount of chloride in the structure. This phenomenon can be explained in terms of a stronger local electrostatic interaction, being Cl more electronegative than Br, and consequently locally "pinning" the mobile Li^+. Next to this, also the volume shrink experienced by the unit cell upon Cl substitution (**Figure 5**) shows the same trend as the activation energy. This is a logical consequence when the conduction pathway is left unchanged but in a smaller volume, the mobile lithium is indeed forced to make the same jump across a smaller bottleneck during its diffusion.

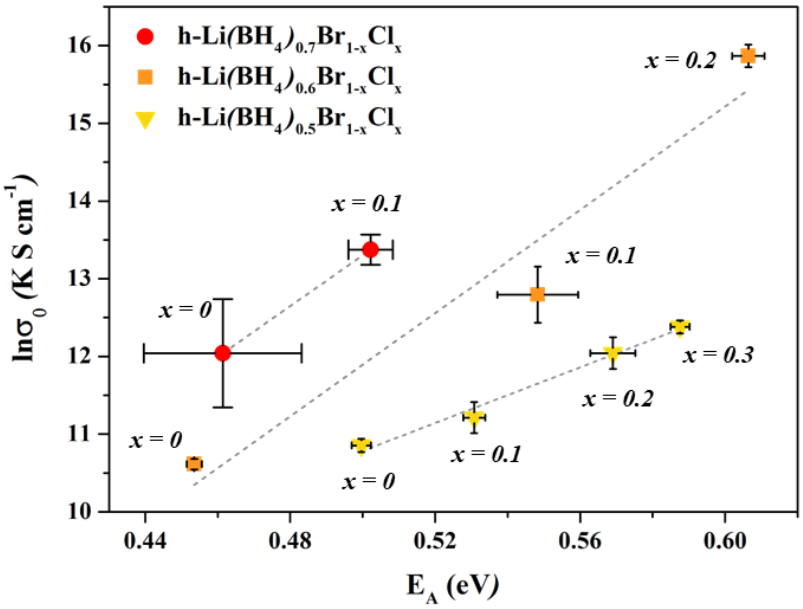

Figure 9. *Plot of the logarithm of the pre-exponential factor ($ln\sigma_0$) as a function of activation energy (E_A) for samples in the hexagonal solid solution for the $LiBH_4$-LiBr-LiCl system. Error bars have been obtained from the linear fit of Arrhenius plot. Dashed lines are a guide for the eyes.*

Figure 10 shows an overview of the electrochemical stability measured at 90 °C as a function of composition, within the monophasic hexagonal solid solution domain. The electrochemical window was established observing the onset of the anodic current at positive potential *vs.* Li^+/Li. Due to the very low current evolving by the electrolyte decomposition that only occurs at the interface, the effective surface area was artificially increased by means of carbon addition as described elsewehere.[74,75] The temperature was set to 90 °C for all compounds (were the conductivity of most of the samples lies above 10^{-5} S/cm) in order to guarantee a low cell resistance (monitored by *in situ* EIS), ensuring the validity of the two-electrodes configuration.

The results shown in **Figure 10** clearly indicate that a deviation of composition from pure $LiBH_4$ involves a reduction of the electrochemical stability window.

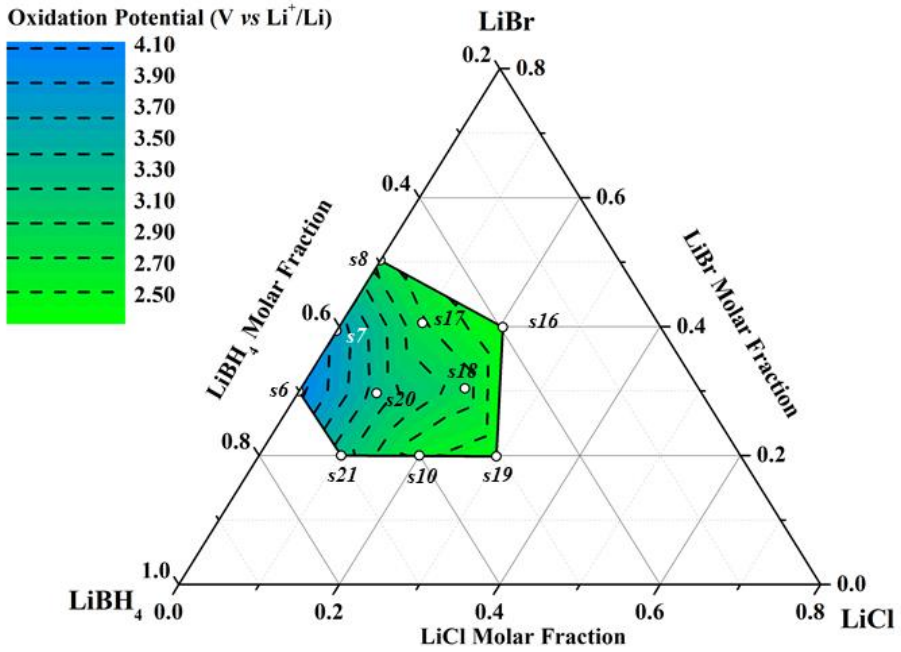

Figure 10. *Contour map of oxidation potential of samples in the hexagonal solid solution in the $LiBH_4$-LiBr-LiCl system as a function of composition, obtained by cyclic voltammetry measured at 90 °C. Iso-potential dashed lines correspond of the values and lines shown in the legend.*

Regarding the binary system $LiBH_4$-LiBr in the studied domain, the oxidative limit systematically lowers with the increasing content of Br^-, moving from a maximum of 4.04 down to 2.85 V for $0.3 < \alpha < 0.5$ ($\beta = 0$). When chloride is added to form a ternary solid solution, the fragility of the system increases, reducing the width of the electrochemical window down to 2.4 V (sample **s16** and **s19**). Nevertheless, a saddle point can be observed in the electrochemical stability map in the phase diagram, when the bromide content is fixed to $\alpha = 0.3$, suggesting an optimum in the composition, less prone to oxidation. It is interesting to note the similar trends in the volume variation as a function of the composition, activation energy for Li^+ mobility and electrochemical window (**Figures 5, 8 and 10**). The dependence of the electrochemical stability from the composition is less straightforward than that of volume and E_A, but can be discussed analysing the decomposition

pathway of pure $LiBH_4$. As already pointed out by the work of Friedrichs *et al.*[76], $LiBH_4$ undergoes hydrogen desorption whilst producing LiH and B_2H_6, the latter further decomposing into B and H_2. Even though the authors stressed that the driving force of such reaction lies on the stability of B_2H_6, it is also worth considering the formation enthalpy of LiH (-90.6 kJ/mol)[77]. In the case of the different solid solutions presented in this work, where Br^- and Cl^- partially replace BH_4^-, a similar decomposition pathway can be inferred. However, LiH would be flanked by the formation of LiBr and LiCl, which are more stable (ΔH_f of -350.9 kJ/mol and -408.7 kJ/mol, respectively)[77]. Consequently, the partial halide replacement affects the electrochemical window, which becomes narrower as the bromide, and more significantly chloride, substitution ratio increases. Nonetheless, a deeper understanding of this effect on the electrochemical stability is necessary and requires further theoretical insight.

To better understand the drop in electrochemical stability upon bromide substitution, with respect these of pure $LiBH_4$, different cross checks were performed on samples **s6** (corresponding to $Li(BH_4)_{0.7}Br_{0.3}$) and pure $LiBH_4$. The CVs were executed at 120 °C, in order to achieve the hexagonal conducting phase of $LiBH_4$.

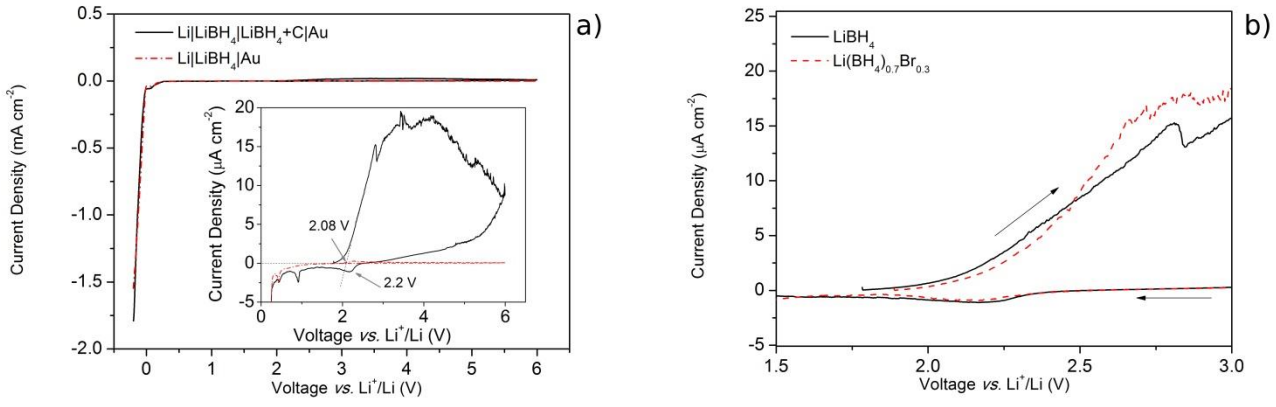

Figure 11. *Cyclic voltammetry measured at 120 °C. a) shows the amplification effect of carbon addition for the small oxidative event; b) compares $LiBH_4$ (continuous lines) and $Li(BH_4)_{0.7}Br_{0.3}$ (dashed lines) in the region 1.5-3.0 V vs. Li^+/Li. The onset of decomposition amounts to 2.26 and 2.08 V for $Li(BH_4)_{0.7}Br_{0.3}$ and $LiBH_4$, respectively.*

Figure 11a shows that the obtained CV for $LiBH_4$ has an electrochemical window of 2.1 V *vs.* Li^+/Li, which is narrower than that reported by Matsuo et al.[15] (5 V *vs.* Li^+/Li). This result could be surprising, but in fact it is in agreement with measurements already shown in literature. In fact, Unemoto *et al.*[78] observed an electrochemical process at 2.1 V, but the authors referred to it as "side-reaction". **Figure 11a** indeed shows to which extent a decomposition process can be hidden by the plating process: the continuous and the dash-dot lines refer to two-layer pellet (with carbon) and simply bulk $LiBH_4$, respectively. The oxidation event, starting at 2.08 V is visible in both measurements, but amplified nearly hundred times by the larger accessible interface thanks to the carbon addition. The other peaks, occurring at low potential, refer to the insertion into graphite (< 0.9 V *vs.* Li^+/Li)[79] and to Li-Au alloying (0.5 V *vs.* Li^+/Li)[80]. It was not possible to identify the cathodic event at 2.2 V, which is however visible only in presence of carbon.

$Li(BH_4)_{0.7}Br_{0.3}$ measured at 120 °C revealed a drop of nearly 1.8 V in its electrochemical window (in **Figure 11b**, compared to pure $LiBH_4$). As it was discussed for conventional carbonate-based electrolyte, the electrochemical window is a thermally activated process,[81] so it is straightforward to justify the depletion of the oxidative stability.

4. Conclusions

In this work, the effect of the anion substitution, promoted by ball milling and thermal treatments, on the Li-ion conductivity in the $LiBH_4$-LiBr-LiCl system has been investigated. For the first time, a ternary hexagonal solid solution containing chloride in the $LiBH_4$ structure was stabilized at *RT* lowering the weight of the electrolyte, therefore increasing the energy density. In addition, the solid solution appears more thermally stable than pure $LiBH_4$ (T_m = 280 °C),[82] as suggested by the absence of the corresponding melting peak in the HP-DSC trace.

The $LiBH_4$-LiBr-LiCl ternary phase diagram has been defined at *RT*, combining XPD data, coupled with a Rietveld refinement and a mass balance. Values of the lattice parameters and volumes of the

hexagonal solid solution have been determined as a function of composition. Because LiCl is immiscible in h-$LiBH_4$ at *RT*, it can be deduced that the presence of Br^- in the solid solution promotes the Cl^- solubilisation, confirming that the dimensions of the anion is a fundamental parameter to be considered. Solubility of up to 30% of Cl^- in the solid solution has been established.

The effect of the composition of the h-$Li(BH_4)_{1-\alpha-\beta}(Br)_\alpha(Cl)_\beta$ solid solution on the Li-ion conductivity has been investigated as a function of temperature using EIS. The h-$Li(BH_4)_{0.7}(Br)_{0.2}(Cl)_{0.1}$ sample showed the highest value of ion conductivity in the ternary solid solution at 30 °C (1.3×10^{-5} S/cm). The chloride anion substitution in the hexagonal structure increases the activation energy but does not affect the Li-ion conductivity; this compensation effect is well described by the Meyer-Neldel rule. Even though such an effect can be explained in terms of lattice stiffening, it is still debated in the literature and either a theoretical model of the phonon spectra modification induced by anion mixing or a direct measure of the speed of sound could shed light on the Li dynamics in investigated complex hydrides.

The destabilization induced by this anion mixing also has a detrimental impact on the electrochemical stability. Taking into account the narrow electrochemical window of $LiBH_4$, the stabilization of the conducting phase at lower temperature (by means of anion substitution) intrinsically increases the electrochemical stability of the solid electrolyte. The effect of the halogenation on the electrochemical stability of the hexagonal solid solution shows that $Li(BH_4)_{0.7}Br_{0.3}$ offers the best electrochemical results, in terms of oxidative stability and Li^+ conductivity and indicates that a deviation of composition involves a reduction of the electrochemical stability window. On the other hand, the ternary phase $Li(BH_4)_{0.7}Br_{0.2}Cl_{0.1}$, although paying a narrower electrochemical window, could offer a 10% gain in weight, with no losses in ionic conductivity.

In summary, the stabilisation at lower temperature of the conductive phase of $LiBH_4$ in this system, not only mitigates the operational temperature of an all-solid-state cell, i.e. increasing the Li ion

conductivity at *RT*, but also enables the use of high-voltage positive electrodes, thus increasing the overall amount of energy stored in the battery. The study of the $LiBH_4$-LiBr-LiCl has shown a flexible system that offers promising candidates for Li-based solid-state electrolytes.

References

(1) Xu, K. Nonaqueous Liquid Electrolytes for Lithium-Based Rechargeable Batteries. *Chem. Rev.* **2004**, *104* (10), 4303–4417.

(2) Bachman, J. C.; Muy, S.; Grimaud, A.; Chang, H.-H.; Pour, N.; Lux, S. F.; Paschos, O.; Maglia, F.; Lupart, S.; Lamp, P.; et al. Inorganic Solid-State Electrolytes for Lithium Batteries: Mechanisms and Properties Governing Ion Conduction. *Chem. Rev.* **2016**, *116* (1), 140–162.

(3) Manthiram, A.; Yu, X.; Wang, S. Lithium Battery Chemistries Enabled by Solid-State Electrolytes. *Nat. Rev. Mater.* **2017**, *2* (4), 16103.

(4) Goodenough, J. B.; Kim, Y. Challenges for Rechargeable Li Batteries †. *Chem. Mater.* **2010**, *22* (3), 587–603.

(5) Tarascon, J.-M.; Armand, M. Issues and Challenges Facing Rechargeable Lithium Batteries. *Nature* **2001**, *414* (6861), 359–367.

(6) Li, W.; Wu, G.; Xiong, Z.; Feng, Y. P.; Chen, P. Li^+ Ionic Conductivities and Diffusion Mechanisms in Li-Based Imides and Lithium Amide. *Phys. Chem. Chem. Phys.* **2012**, *14* (5), 1596–1606.

(7) Boukamp, B. A.; Huggins, R. A. Ionic Conductivity in Lithium Imide. *Phys. Lett. A* **1979**, *72* (6), 464–466.

(8) Kanno, R.; Hata, T.; Kawamoto, Y.; Irie, M. Synthesis of a New Lithium Ionic Conductor, Thio-LISICON-Lithium Germanium Sulfide System. *Solid State Ionics* **2000**, *130* (1), 97–104.

(9) Stramare, S.; Thangadurai, V.; Weppner, W. Lithium Lanthanum Titanates: A Review. *Chem. Mater.* **2003**, *15* (21), 3974–3990.

(10) Inaguma, Y.; Liquan, C.; Itoh, M.; Nakamura, T.; Uchida, T.; Ikuta, H.; Wakihara, M. High Ionic Conductivity in Lithium Lanthanum Titanate. *Solid State Commun.* **1993**, *86* (10), 689–693.

(11) Tan, J.; Tiwari, A. LLZO Synthesis of Cubic Phase $Li_7La_3Zr_2O_{12}$ Electrolyte for Solid-State Lithium-Ion Batteries. *Electrochem. Solid-State Lett.* **2012**, *15* (3), A37.

(12) Sanjuán, M. L.; Laguna, M. A.; Belous, A. G.; V'yunov, O. I. On the Local Structure and Lithium Dynamics of $La_{0.5}(Li,Na)_{0.5}TiO_3$ Ionic Conductors. A Raman Study. *Chem. Mater.* **2005**, *17* (23), 5862–5866.

(13) Ortiz, G. F.; López, M. C.; Lavela, P.; Vidal-Abarca, C.; Tirado, J. L. Improved Lithium-Ion Transport in NASICON-Type Lithium Titanium Phosphate by Calcium and Iron Doping. *Solid State Ionics* **2014**, *262*, 573–577.

(14) Deng, Y.; Eames, C.; Nguyen, L. H. B.; Pecher, O.; Griffith, K. J.; Courty, M.; Fleutot, B.; Chotard, J.-N.; Grey, C. P.; Islam, M. S.; et al. Crystal Structures, Local Atomic Environments, and Ion Diffusion Mechanisms of Scandium-Substituted Sodium Superionic Conductor (NASICON) Solid Electrolytes. *Chem. Mater.* **2018**, *30*

(8), 2618–2630.

(15) Matsuo, M.; Orimo, S. Lithium Fast-Ionic Conduction in Complex Hydrides: Review and Prospects. *Adv. Energy Mater.* **2011**, *1* (2), 161–172.

(16) Duchêne, L.; Kühnel, R.-S.; Stilp, E.; Cuervo Reyes, E.; Remhof, A.; Hagemann, H.; Battaglia, C. A Stable 3 V All-Solid-State Sodium–Ion Battery Based on a Closo -Borate Electrolyte. *Energy Environ. Sci.* **2017**, *10* (12), 2609–2615.

(17) Unemoto, A.; Yoshida, K.; Ikeshoji, T.; Orimo, S. Bulk-Type All-Solid-State Lithium Batteries Using Complex Hydrides Containing Cluster-Anions. *Mater. Trans.* **2016**, *57* (9), 1639–1644.

(18) Tang, W. S.; Unemoto, A.; Zhou, W.; Stavila, V.; Matsuo, M.; Wu, H.; Orimo, S. I.; Udovic, T. J. Unparalleled Lithium and Sodium Superionic Conduction in Solid Electrolytes with Large Monovalent Cage-like Anions. *Energy Environ. Sci.* **2015**, *8* (12), 3637–3645.

(19) Soulie, J.; Renaudin, G.; Černý, R.; Yvon, K. Lithium Boro-Hydride $LiBH_4$ I. Crystal Structure. *J. Alloys Compd.* **2002**, *346*, 200–205.

(20) Matsuo, M.; Nakamori, Y.; Orimo, S.; Maekawa, H.; Takamura, H. Lithium Superionic Conduction in Lithium Borohydride Accompanied by Structural Transition. *Appl. Phys. Lett.* **2007**, *91* (22), 224103.

(21) Goodenough, J. B.; Park, K. The Li-Ion Rechargeable Battery: A Perspective. *J. Am. Chem. Soc.* **2013**, *135* (4), 1167–1176.

(22) Park, M.; Zhang, X.; Chung, M.; Less, G. B.; Sastry, A. M. A Review of Conduction Phenomena in Li-Ion Batteries. *J. Power Sources* **2010**, *195* (24), 7904–7929.

(23) Jansen, M. Volume Effect or Paddle-Wheel Mechanism-Fast Alkali-Metal Ionic Conduction in Solids with Rotationally Disordered Complex Anions. *Angew. Chemie Int. Ed. English* **1991**, *30* (12), 1547–1558.

(24) C.Kittel. *Introduction to Solid State Physics*; Wiley, Ed.; 2005.

(25) Lee, Y.-S.; Cho, Y. W. Fast Lithium Ion Migration in Room Temperature $LiBH_4$. *J. Phys. Chem. C* **2017**, *121* (33), 17773–17779.

(26) Goodenough, J. B. Oxide-Ion Electrolytes. *Annu. Rev. Mater. Res.* **2003**, *33* (1), 91–128.

(27) Goodenough, J. B. Review Lecture: Fast Ionic Conduction in Solids. *Proc. R. Soc. A Math. Phys. Eng. Sci.* **1984**, *393* (1805), 215–234.

(28) Wolczyk, A.; Pinatel, E. R.; Chierotti, M. R.; Nervi, C.; Gobetto, R.; Baricco, M. Solid-State NMR and Thermodynamic Investigations on $LiBH_4LiNH_2$ System. *Int. J. Hydrogen Energy* **2016**, *41* (32), 14475–14483.

(29) Davies, R. A.; Hewett, D. R.; Anderson, P. A. Enhancing Ionic Conductivity in Lithium Amide for Improved Energy Storage Materials. *Adv. Nat. Sci. Nanosci. Nanotechnol.* **2015**, *6* (1), 015005.

(30) Matsuo, M.; Remhof, A.; Martelli, P.; Caputo, R.; Ernst, M.; Miura, Y.; Sato, T.; Oguchi, H.; Maekawa, H.; Takamura, H.; et al. Complex Hydrides with $(BH_4)^-$ and $(NH_2)^-$ Anions as New Lithium Fast-Ion Conductors. *J. Am. Chem. Soc.* **2009**, *131* (45), 16389–16391.

(31) Paskevicius, M.; Jepsen, L. H.; Schouwink, P.; Černý, R.; Ravnsbæk, D. B.; Filinchuk, Y.; Dornheim, M.; Besenbacher, F.; Jensen, T. R. Metal Borohydrides and Derivatives – Synthesis, Structure and Properties. *Chem. Soc. Rev.* **2017**, *46* (5), 1565–1634.

(32) Sveinbjörnsson, D.; Myrdal, J. S. G.; Blanchard, D.; Bentzen, J. J.; Hirata, T.; Mogensen, M. B.; Norby, P.; Orimo, S.; Vegge, T. Effect of Heat Treatment on the Lithium Ion Conduction of the $LiBH_4$–LiI Solid Solution. *J. Phys. Chem. C* **2013**, *117* (7), 3249–3257.

(33) Yao, Z.; Kim, S.; Michel, K.; Zhang, Y.; Aykol, M.; Wolverton, C. Stability and Conductivity of Cation- and Anion-Substituted $LiBH_4$ -Based Solid-State Electrolytes. *Phys. Rev. Mater.* **2018**, *2* (6), 37–39.

(34) Miyazaki, R.; Karahashi, T.; Kumatani, N.; Noda, Y.; Ando, M.; Takamura, H.; Matsuo, M.; Orimo, S.; Maekawa, H. Room Temperature Lithium Fast-Ion Conduction and Phase Relationship of LiI Stabilized $LiBH_4$. *Solid State Ionics* **2011**, *192* (1), 143–147.

(35) Cascallana-Matias, I.; Keen, D. A.; Cussen, E. J.; Gregory, D. H. Phase Behavior in the $LiBH_4$–LiBr System and Structure of the Anion-Stabilized Fast Ionic, High Temperature Phase. *Chem. Mater.* **2015**, *27* (22), 7780–7787.

(36) Zhou, Y.; Matsuo, M.; Miura, Y.; Takamura, H.; Maekawa, H.; Remhof, A.; Borgschulte, A.; Züttel, A.; Otomo, T.; Orimo, S. Enhanced Electrical Conductivities of Complex Hydrides $Li_2(BH_4)(NH_2)$ and $Li_4(BH_4)(NH_2)_3$ by Melting. *Mater. Trans.* **2011**, *52* (4), 654–657.

(37) Choi, Y. S.; Lee, Y.-S.; Oh, K. H.; Cho, Y. W. Interface-Enhanced Li Ion Conduction in a $LiBH_4$-SiO_2 Solid Electrolyte. *Phys. Chem. Chem. Phys.* **2016**, *18* (32), 22540–22547.

(38) Choi, Y. S.; Lee, Y.-S.; Choi, D.-J.; Chae, K. H.; Oh, K. H.; Cho, Y. W. Enhanced Li Ion Conductivity in $LiBH_4$–Al_2O_3 Mixture via Interface Engineering. *J. Phys. Chem. C* **2017**, *121* (47), 26209–26215.

(39) Lefevr, J.; Cervini, L.; Griffin, J. M.; Blanchard, D. Lithium Conductivity and Ions Dynamics in $LiBH_4/SiO_2$ Solid Electrolytes Studied by Solid-State NMR and Quasi-Elastic Neutron Scattering and Applied in Lithium–Sulfur Batteries. *J. Phys. Chem. C* **2018**, *122* (27), 15264–15275.

(40) Blanchard, D.; Nale, A.; Sveinbjörnsson, D.; Eggenhuisen, T. M.; Verkuijlen, M. H. W.; Suwarno; Vegge, T.; Kentgens, A. P. M.; de Jongh, P. E. Nanoconfined $LiBH_4$ as a Fast Lithium Ion Conductor. *Adv. Funct. Mater.* **2015**, *25* (2), 184–192.

(41) Tian, Y.; Shi, T.; Richards, W. D.; Li, J.; Kim, J. C.; Bo, S.-H.; Ceder, G. Compatibility Issues between Electrodes and Electrolytes in Solid-State Batteries. *Energy Environ. Sci.* **2017**, *10* (5), 1150–1166.

(42) J. Sangster, A. P. Phase Diagrams and Thermodynamic Properties of the 70 Binary Alkali Halide Systems Having Common Ions. *J. Phys. Chem. C* **1987**, *16*, 511–561.

(43) Lutterotti, L., Matthies, S., Wenk, H. R. MAUD: A Friendly Java Program for Material Analysis Using Diffraction. *MAUD A Friendly Java Progr. Mater. Anal. Using Diffr.* **1999**, 14–15.

(44) Boukamp, B. A. Electrochemical Impedance Spectroscopy in Solid State Ionics: Recent Advances. *Solid State Ionics* **2004**, *169* (1-4 SPEC. ISS.), 65–73.

(45) Boukamp, B. A. A Package for Impedance/Admittance Data Analysis. *Solid State Ionics* **1986**, *19*, 136–140.

(46) Oguchi, H.; Matsuo, M.; Hummelshøj, J. S.; Vegge, T.; Nørskov, J. K.; Sato, T.; Miura, Y.; Takamura, H.; Maekawa, H.; Orimo, S. Experimental and Computational Studies on Structural Transitions in the $LiBH_4$–LiI Pseudobinary System. *Appl. Phys. Lett.* **2009**, *94* (14), 141912.

(47) Filinchuk, Y.; Chernyshov, D.; Cerny, R. Lightest Borohydride Probed by Synchrotron X-Ray Diffraction: Experiment Calls for a New Theoretical Revision. *J. Phys. Chem. C* **2008**, *112* (28), 10579–10584.

(48) Shannon, R. D. Revised Effective Ionic Radii and Systematic Studies of Interatomic Distances in Halides and Chalcogenides. *Acta Crystallogr. Sect. A* **1976**, *32* (5), 751–767.

(49) Abrahams, S. C.; Kalnajs, J. The Lattice Constants of the Alkali Borohydrides and the Low-Temperature Phase of Sodium Borohydride. *J. Chem. Phys.* **1954**, *22* (3), 434–436.

(50) Černý, R.; Schouwink, P. The Crystal Chemistry of Inorganic Metal Boro-Hydrides and Their Relation to Metal Oxides. *Acta Crystallogr. Sect. B Struct. Sci. Cryst. Eng. Mater.* **2015**, *71*, 619–640.

(51) Pistorius, C. W. F. T. Melting and Polymorphism of $LiBH_4$ to 45 Kbar. *Z. Phys. Chem. Neue Folge* **1974**, *88*, 253–263.

(52) Rude, L. H.; Zavorotynska, O.; Arnbjerg, L. M.; Ravnsbæk, D. B.; Malmkjær, R. A.; Grove, H.; Hauback, B. C.; Baricco, M.; Filinchuk, Y.; Besenbacher, F.; et al. Bromide Substitution in Lithium Borohydride, $LiBH_4$–LiBr. *Int. J. Hydrogen Energy* **2011**, *36* (24), 15664–15672.

(53) Tomkinson, J.; Waddington, T. C. Inelastic Neutron Scattering from the Alkali Metal Borohydrides and Calcium Borohydride. *J. Chem. Soc. Faraday Trans. 2* **1976**, *72*, 528.

(54) Hagemann, H.; Gomes, S.; Renaudin, G.; Yvon, K. Raman Studies of Reorientation Motions of $[BH_4]^-$ Anionsin Alkali Borohydrides. *J. Alloys Compd.* **2004**, *363* (1–2), 129–132.

(55) D'Anna, V.; Spyratou, A.; Sharma, M.; Hagemann, H. FT-IR Spectra of Inorganic Borohydrides. *Spectrochim.*

Acta Part A Mol. Biomol. Spectrosc. **2014**, *128*, 902–906.

(56) Hagemann, H.; Filinchuk, Y.; Chernyshov, D.; Van Beek, W. Lattice Anharmonicity and Structural Evolution of $LiBH_4$: An Insight from Raman and X-Ray Diffraction Experiments. *Phase Transitions* **2009**, *82* (4), 344–355.

(57) Rude, L. H.; Groppo, E.; Arnbjerg, L. M.; Ravnsbæk, D. B.; Malmkjær, R. A.; Filinchuk, Y.; Baricco, M.; Besenbacher, F.; Jensen, T. R. Iodide Substitution in Lithium Borohydride, $LiBH_4$–LiI. *J. Alloys Compd.* **2011**, *509* (33), 8299–8305.

(58) GharibDoust, S. H. P.; Brighi, M.; Sadikin, Y.; Ravnsbæk, D. B.; Černý, R.; Skibsted, J.; Jensen, T. R. Synthesis, Structure, and Li-Ion Conductivity of $LiLa(BH_4)_3X$, X = Cl, Br, I. *J. Phys. Chem. C* **2017**, *121* (35), 19010–19021.

(59) Davies, P. K.; Navrotsky, A. Quantitative Correlations of Deviations from Ideality in Binary and Pseudobinary Solid Solutions. *J. Solid State Chem.* **1983**, *46* (1), 1–22.

(60) Zavorotynska, O.; Corno, M.; Pinatel, E.; Rude, L. H.; Ugliengo, P.; Jensen, T. R.; Baricco, M. Theoretical and Experimental Study of $LiBH_4$-LiCl Solid Solution. *Crystals* **2012**, *2* (4), 144–158.

(61) Morse, S. A. Binary Solutions and the Lever Rule Revisited. *J. Geol.* **1997**, *105* (4), 471–482.

(62) Kraft, M. A.; Culver, S. P.; Calderon, M.; Böcher, F.; Krauskopf, T.; Senyshyn, A.; Dietrich, C.; Zevalkink, A.; Janek, J.; Zeier, W. G. Influence of Lattice Polarizability on the Ionic Conductivity in the Lithium Superionic Argyrodites Li_6PS_5X (X = Cl, Br, I). *J. Am. Chem. Soc.* **2017**, *139* (31), 10909–10918.

(63) Krauskopf, T.; Pompe, C.; Kraft, M. A.; Zeier, W. G. Influence of Lattice Dynamics on Na+Transport in the Solid Electrolyte $Na_3PS_{4-x}Se_x$. *Chem. Mater.* **2017**, *29* (20), 8859–8869.

(64) E. Barsoukov, J. R. M. *Impedance Spectroscopy: Theory, Experiment, and Applications*, Wiley and.; 2005.

(65) Buchter, F.; Łodziana, Z.; Mauron, P.; Remhof, A.; Friedrichs, O.; Borgschulte, A.; Züttel, A.; Sheptyakov, D.; Strässle, T.; Ramirez-Cuesta, A. J. Dynamical Properties and Temperature Induced Molecular Disordering of $LiBH_4$ and $LiBD_4$. *Phys. Rev. B* **2008**, *78* (9), 094302.

(66) Martelli, P.; Remhof, A.; Borgschulte, A.; Ackermann, R.; Strässle, T.; Embs, J. P.; Ernst, M.; Matsuo, M.; Orimo, S.; Züttel, A. Rotational Motion in $LiBH_4$ /LiI Solid Solutions. *J. Phys. Chem. A* **2011**, *115* (21), 5329–5334.

(67) Tilley, R. J. D. *Defects in Solids*, 10th ed.; John Wiley & Sons, Ed.; 2008.

(68) Altshuller, A. P. Lattice Energies and Related Thermodynamic Properties of the Alkali Metal Borohydrides and of the Borohydride Ion. *J. Am. Chem. Soc.* **1955**, *77* (21), 5455–5457.

(69) Viščor, P. Comment on "Origin and Consequences of the Compensation (Meyer-Neldel) Law." *Phys. Rev. B* **2002**, *65* (7), 077201.

(70) Krauskopf, T.; Culver, S. P.; Zeier, W. G. Bottleneck of Diffusion and Inductive Effects in $Li_{10}Ge_{1-x}Sn_xP_2S_{12}$. *Chem. Mater.* **2018**, *30* (5), 1791–1798.

(71) Culver, S. P.; Koerver, R.; Krauskopf, T.; Zeier, W. G. Designing Ionic Conductors: The Interplay between Structural Phenomena and Interfaces in Thiophosphate-Based Solid-State Batteries. *Chem. Mater.* **2018**, *30* (13), 4179–4192.

(72) Yelon, A.; Movaghar, B. Reply to "Comment on 'Origin and Consequences of the Compensation (Meyer-Neldel) Law' ." *Phys. Rev. B* **2002**, *65* (7), 077202.

(73) Gremaud, R.; Züttel, A.; Borgschulte, A.; Ramirez-cuesta, A. J.; Refson, K.; Colognesi, D. Origin of the Large Anharmonicity in the Phonon Modes of $LiBH_4$. *Chem. Phys.* **2013**, *427*, 22–29.

(74) Han, F.; Zhu, Y.; He, X.; Mo, Y.; Wang, C. Electrochemical Stability of $Li_{10}GeP_2S_{12}$ and $Li_7La_3Zr_2O_{12}$ Solid Electrolytes. *Adv. Energy Mater.* **2016**, *6* (8), 1501590.

(75) Brighi, M.; Murgia, F.; Łodziana, Z.; Schouwink, P.; Wołczyk, A.; Cerny, R. A Mixed Anion Hydroborate / Carba-Hydroborate as a Room Temperature Na- Ion Solid Electrolyte. *J. Power Sources* **2018**, *404* (August), 7–12.

(76) Friedrichs, O.; Remhof, A.; Hwang, S.-J.; Züttel, A. Role of $Li_2B_{12}H_{12}$ for the Formation and Decomposition of LiBH4. *Chem. Mater.* **2010**, *22* (10), 3265–3268.

(77) Chase, M. W. *NIST-JANAF Thermochemical Tables*, 4th editio.; [Washington, D.C.]: American Chemical Society, 1998.

(78) Unemoto, A.; Ikeshoji, T.; Yasaku, S.; Matsuo, M.; Stavila, V.; Udovic, T. J.; Orimo, S. Stable Interface Formation between TiS_2 and $LiBH_4$ in Bulk-Type All-Solid-State Lithium Batteries. *Chem. Mater.* **2015**, *27* (15), 5407–5416.

(79) Yazami, R.; Touzain, P. A Reversible Graphite-Lithium Electrochemical Generators. *J. Power Sources* **1983**, *9*, 365–371.

(80) F.U. Renner, H. Kageyama, Z. Siroma, M. Shikano, S. Schoder, Y. Grunder, O. S. Electrochimica Acta Gold Model Anodes for Li-Ion Batteries : Single Crystalline Systems Studied by in Situ X-Ray Diffraction. *Electrochim. Acta* **2008**, *53*, 6064–6069.

(81) Turk, M. C.; Johnson, C. A.; Roy, D. Electroanalytical Evaluation of Temperature Dependent Electrolyte Functions for Lithium Ion Batteries : Investigation of Selected Mixed Carbonate Solvents Using a Lithium Titanate Electrode. *J. Energy Storage* **2018**, *20* (September), 395–408.

(82) El Kharbachi, A.; Pinatel, E.; Nuta, I.; Baricco, M. A Thermodynamic Assessment of $LiBH_4$. *Calphad* **2012**, *39*, 80–90.